International Information and Engineering Technology Association
Advancing the World of Information and Engineering

Revue des Composites et des Matériaux Avancés-Journal of Composite and Advanced Materials
Vol. 36, No. 4, August, 2026, pp. 859-876
Journal homepage: http://iieta.org/journals/rcma

Piezoelectric Materials for Autonomous Internet of Things and Edge Intelligence: From Fundamental Physics to Self-Powered Intelligent Systems

Bachar Mourched[1*], Mariam Abdallah[2]

[1] College of Engineering and Technology, American University of the Middle East, Egaila 54200, Kuwait
[2] Faculty of Science III, Lebanese University, Tripoli 6573, Lebanon

Corresponding Author Email: bachar.mourched@aum.edu.kw

https://doi.org/10.18280/rcma.360415

Received: 6 June 2026
Revised: 27 July 2026
Accepted: 12 August 2026
Available online: 31 August 2026

Keywords:
piezoelectric materials, self-powered sensors, energy harvesting, edge AI, TinyML, flexible electronics, nanogenerators, autonomous Internet of Things systems

ABSTRACT

Piezoelectric materials have evolved from simple electromechanical transducers into key enablers of autonomous sensing systems. With the expansion of Internet of Things (IoT) applications, the challenge is no longer maximizing material coefficients alone but achieving sustained operation under strict energy constraints. This review presents a system-level perspective linking piezoelectric physics, material classes, device fabrication, power-management electronics, and embedded machine learning within a unified autonomy framework. After summarizing polarization mechanisms across ceramics, polymers, composites, and nanoscale structures, the discussion connects intrinsic coefficients to extractable electrical energy through interface efficiency and storage losses. A quantitative energy-balance condition is introduced to show how sensing, inference, and wireless communication jointly determine energy feasibility and the autonomy margin. The analysis shows that, in communication-dominated systems, local inference and event-driven transmission can provide greater autonomy gains than incremental improvements in piezoelectric response. Recent advances in lead-free ceramics, flexible polyvinylidene fluoride (PVDF) systems, hybrid harvesters, and edge-AI architectures demonstrate the feasibility of self-powered intelligent nodes, while remaining challenges include long-term reliability, variable excitation environments, and reproducible benchmarking. The review establishes that autonomous piezoelectric sensing is fundamentally an energy-information co-design problem, providing practical guidelines for designing scalable, self-sustaining IoT networks.

1. INTRODUCTION

The rapid proliferation of Internet of Things (IoT) technologies is transforming modern infrastructure, healthcare, transportation, and environmental monitoring into interconnected cyber-physical ecosystems. Billions of distributed sensor nodes are expected to operate in locations where wired power is unavailable and battery replacement is impractical, making energy autonomy a primary barrier to large-scale deployment. Conventional sensing platforms remain constrained by the energy required for acquisition, processing, and wireless communication, motivating sensing mechanisms capable of both detecting events and powering their own electronics.

Among ambient energy sources, mechanical energy is particularly attractive because it is ubiquitous in natural and built environments: structural vibrations, human motion, airflow, acoustic waves, and pressure fluctuations are continuously present across multiple scales. Piezoelectric materials are uniquely suited to exploit this resource because they inherently couple mechanical and electrical domains, allowing direct conversion of mechanical deformation into electrical charge while simultaneously acting as sensing elements. This dual functionality distinguishes piezoelectric systems from other energy harvesters and positions them as a key enabling technology for self-powered sensing architectures.

The understanding of piezoelectricity evolved from early electromechanical observations in quartz crystals [1, 2] to engineered sonar transducers [3], and later to optimized ferroelectric ceramics forming the basis of modern electromechanical devices [4, 5]. Ferroelectric ceramics such as barium titanate and lead zirconate titanate (PZT) enabled high coupling coefficients and industrial reliability [6], while the discovery of piezoelectric polymers such as polyvinylidene fluoride (PVDF) introduced flexibility and large-area conformability [7]. More recently, nanoscale and two-dimensional materials including ZnO nanowires and halide perovskites have demonstrated electromechanical coupling at extremely small thicknesses [8], alongside the development of environmentally friendly lead-free compositions. As a result, piezoelectric technology has evolved from simple transducers to multifunctional platforms capable of sensing, actuation, and energy harvesting.

Mechanical energy harvesting using piezoelectric structures has been demonstrated for powering wireless and mobile electronics [9, 10]. Nonlinear and bi-stable piezoelectric configurations have also been investigated to improve energy-harvesting performance over varying excitation conditions [11], while electromechanical architectures integrating piezoelectric elements with vibration and wave-control structures provide another route for converting captured mechanical energy into electrical power [12]. Biomedical systems that harvest energy from cardiac and respiratory motion have further shown the feasibility of extending implant lifetime [13]. However, increasing material performance alone does not guarantee autonomous operation. In practical IoT nodes, wireless communication and data processing often dominate the energy budget, making system architecture as important as the material itself. Recent advances in ultra-low-power computing and tiny machine learning (TinyML) enable local interpretation of sensor signals, dramatically reducing transmission requirements [14-16].

At the same time, scalable deployment requires compatible fabrication processes and long-term durability. Manufacturing pathways compatible with flexible substrates and integrated electronics are actively being explored [6], while long-term reliability under cyclic loading and environmental exposure remains a major challenge requiring fatigue-aware design and encapsulation strategies [17]. Hybrid and stacked harvesting architectures have been proposed to extend operation under variable excitation conditions [18], and recent demonstrations confirm that piezoelectric devices can function simultaneously as sensors and energy sources in realistic IoT platforms [19].

Despite rapid progress across materials, fabrication, power electronics, and machine learning, these advances are typically optimized in isolation. As a result, reported improvements in piezoelectric coefficients or harvested power do not necessarily translate into longer operational lifetime. Autonomous sensing is instead governed by the balance between generated energy, conversion efficiency, and algorithmic cost—a balance that remains insufficiently addressed in existing literature. While recent reviews comprehensively cover either material synthesis and harvesting circuits, or energy-harvesting technologies more broadly, they do not explicitly formulate the energy-information co-design condition linking material, circuit, and algorithmic layers that this work addresses.

Accordingly, this review provides an integrated perspective linking material physics, fabrication constraints, power-management efficiency, and embedded intelligence within a unified energy-autonomy framework. The energy-balance relation used in this framework is not proposed as a new conservation law. Its contribution is a design-oriented cross-layer interpretation that expresses material-dependent energy generation, interface losses, sensing and inference costs, communication frequency, and standby losses using a common autonomy criterion. This formulation enables interventions at different system layers — for example, increasing piezoelectric output or reducing radio activity—to be compared quantitatively rather than discussed independently. Specifically, the work (i) connects intrinsic coefficients (e.g., d_{33}, g_{33}) to extractable electrical energy, (ii) classifies materials by functional suitability for autonomous nodes, (iii) analyzes harvesting and duty-cycled operation in the context of system power budgets, and (iv) consolidates TinyML-based sensing strategies into deployable architectures.

This review adopts a narrative approach to synthesize interdisciplinary advances spanning piezoelectric materials, energy harvesting circuits, and embedded machine learning for autonomous IoT systems. The literature search was conducted primarily through Scopus, Web of Science, and IEEE Xplore, supplemented by Google Scholar for cross-referencing and grey literature identification. The search employed combinations of the following keyword strings: *"piezoelectric energy harvesting," "self-powered sensor," "piezoelectric IoT," "TinyML," "edge AI," "lead-free piezoceramics," "nanogenerator," "PVDF sensor," "power management harvesting,"* and *"autonomous sensing"*. The search covered publications from 2000 to 2026, with priority given to peer-reviewed journal articles, foundational textbooks, and high-impact conference proceedings. Earlier seminal works (pre-2000) were included where necessary to establish historical context and foundational principles. No formal inclusion/exclusion scoring rubric was applied, consistent with the narrative review methodology; however, source selection prioritized: (a) studies reporting quantitative electromechanical or energy-harvesting performance data, (b) works demonstrating system-level integration of sensing and intelligence, and (c) recent comprehensive reviews used for cross-validation and positioning. Reference lists of key review articles were manually screened (backward citation tracking) to identify additional relevant studies. In total, approximately 250 sources were screened, of which 80 are cited in this work.

The remainder of the paper first reviews the physical principles governing piezoelectric coupling, followed by the evolution of material systems from ceramics to nanostructures. Fabrication and characterization methods are then discussed, after which system-level integration with IoT architectures and edge intelligence is analyzed. Finally, challenges and future research directions are presented, outlining the pathway toward scalable, long-term, self-powered sensing networks.

2. FUNDAMENTAL PRINCIPLES OF PIEZOELECTRICITY

Piezoelectricity arises from the intrinsic coupling between mechanical and electrical states in non-centrosymmetric materials. When mechanical stress distorts the crystal lattice, a displacement of positive and negative charge centers generates electric polarization; conversely, an applied electric field induces mechanical strain. This bidirectional electromechanical interaction, first experimentally demonstrated by the Curie brothers [1] and theoretically anticipated by Lippmann [2], defines the operational basis of sensors, actuators, and energy harvesters. Crystallographic analysis later established that only specific symmetry classes permit this coupling, with a subset exhibiting ferroelectric behavior characterized by reversible spontaneous polarization [20].

2.1 Constitutive electromechanical relations

At the continuum scale, piezoelectric behavior is described by linear constitutive equations coupling mechanical and electrical variables. In strain-charge form, the relations are shown in Eqs. (1) and (2).

$$S = s^E T + d^t E \tag{1}$$

$$D = dT + \varepsilon^T E \quad (2)$$

where, S is the strain vector, T is the stress vector, E is the electric field, D is the electric displacement, s^E is the elastic compliance at constant electric field, ε^T is the permittivity at constant stress, and d is the piezoelectric coefficient matrix quantifying the electromechanical coupling strength [5].

These relations describe the converse effect (Eq. (1)) and the direct effect (Eq. (2)), respectively.

In practice, materials are characterized using scalar performance parameters such as the longitudinal coefficient d_{33}, transverse coefficient d_{31}, voltage constant g_{ij}, electromechanical coupling factor k, and mechanical quality factor Q, which determine sensitivity, conversion efficiency, and resonant behavior [21, 22].

2.2 Polarization mechanisms and material response

The magnitude of piezoelectric response varies widely depending on the polarization mechanism. In stable crystals such as quartz, polarization arises from small ionic displacement and therefore produces limited electrical output. In contrast, ferroelectric ceramics exhibit large responses because polarization occurs through domain switching, where dipoles reorient collectively under mechanical or electrical loading [23].

Recent studies emphasize that macroscopic piezoelectric performance is governed not only by intrinsic lattice polarization but also by the mobility and interaction of domain walls. Grain size, crystallographic texture, porosity, defect chemistry, and local mechanical constraints can either enhance or suppress domain-wall motion, thereby modifying dielectric, piezoelectric, and electromechanical properties [24].

Macroscopic coefficients are commonly measured using quasi-static loading methods such as the Berlincourt technique [25], while resonance-antiresonance analysis provides dynamic coupling parameters. At smaller scales, piezoresponse force microscopy enables direct visualization of polarization domains and switching behavior, revealing heterogeneities that strongly influence device performance [26].

2.3 Microscopic origin and stability

At the microscopic level, piezoelectricity originates from symmetry-breaking displacement of charge centers within the crystal lattice. In perovskite ferroelectrics, polarization is produced by displacement of the central cation relative to surrounding oxygen octahedra [27]. The evolution of polarization under electric field or mechanical stress is described by Landau-Devonshire theory, explaining hysteresis and phase transitions [28]. Over long-term operation, domain-wall motion and defect dipoles cause aging and fatigue, gradually degrading the electromechanical response [29].

In addition to classical piezoelectricity, strong strain gradients can induce polarization even in centrosymmetric materials, a phenomenon known as flexoelectricity, expanding the theoretical framework of electromechanical coupling [30].

Because different applications prioritize different electromechanical figures of merit, comparing multiple coefficients is more informative than considering a single parameter alone. In particular, the charge coefficient d_{33} reflects actuation capability, whereas the voltage coefficient g_{33} governs sensing sensitivity in high-impedance systems. Table 1 summarizes representative performance indicators for common piezoelectric materials and highlights the fundamental trade-off between charge generation, voltage output, and mechanical compliance.

Table 1. Representative piezoelectric coefficients and performance indicators for common material systems, compiled from the cited literature

Material	d_{33} (pC/N)	$g_{33} \times 10^{-3}$ (V·m/N)	k_{33}	Key Feature
Quartz [20, 21]	2.3	13	0.10	Chemically stable, low output
Lead zirconate titanate (PZT) [21, 22, 31, 32]	300–600	12–20	0.70	High coupling, brittle
Polyvinylidene fluoride (PVDF) [7, 21, 33]	20–30	216	0.20	Flexible, low permittivity
ZnO nanowires [34, 35]	8–15	120	0.35	Nanoscale generators

Note that the values are representative of the cited literature and may vary with composition, crystal orientation, processing, poling conditions, measurement frequency, mechanical boundary conditions, and characterization method. Values reported for nanoscale structures should not be compared directly with bulk-material coefficients unless equivalent definitions and measurement conditions are used.

Reported coefficients depend strongly on processing route, poling condition, frequency, and measurement method; therefore, the values in Table 1 represent typical ranges rather than absolute limits. As shown in Table 1, ferroelectric ceramics such as PZT exhibit very large d_{33} and coupling factors, making them suitable for actuation and ultrasonic transduction but mechanically rigid. In contrast, PVDF displays a much higher voltage coefficient g_{33} despite lower charge generation, explaining its effectiveness in wearable and low-power sensing applications. Nanoscale materials such as ZnO nanowires provide intermediate performance while enabling miniaturization and mechanical compliance. This comparison demonstrates that piezoelectric material selection depends primarily on application requirements rather than maximizing a single coefficient, a concept central to IoT-oriented sensor design [24].

2.4 Implications of d_{33}, g_{33}, and device capacitance for Internet of Things sensing

While d_{33} is often used to compare the charge-generation capability of piezoelectric materials, IoT sensing and energy harvesting are also strongly influenced by voltage response, impedance matching, and effective device capacitance. In high-impedance readout circuits typical of low-power microcontrollers, the voltage response depends strongly on the piezoelectric voltage coefficient g_{ij} and dielectric permittivity. This explains why polymer systems can remain competitive for sensing despite having lower d_{33} values. Conversely, harvesting interfaces must extract energy from a predominantly capacitive source with limited current capability. A material may therefore appear highly effective in coefficient tables yet provide limited net usable energy when rectification, leakage, storage, and impedance-matching losses are considered.

These material parameters can be connected directly to the harvested-power term used in the system-level autonomy condition. For a force-driven piezoelectric element operating through the direct piezoelectric effect, the generated charge can be approximated as:

$$Q = d_{\mathrm{eff}} F$$

where, d_{eff} is the effective piezoelectric coefficient for the selected electromechanical mode and device orientation, and F is the force transferred to the active material. The maximum electrostatic energy stored in the effective piezoelectric capacitance at the voltage peak can then be approximated as [21].

$$E_{\mathrm{elec,max}} \approx \frac{Q^2}{2C_p} = \frac{d_{\mathrm{eff}}^2 F^2}{2C_p}$$

where, C_p is the effective capacitance of the piezoelectric element. If one effective energy-extraction event occurs per excitation cycle, an idealized upper-bound scaling for the average transducer power is:

$$P_{\mathrm{harv,ideal}} \approx f_{\mathrm{exc}} E_{\mathrm{elec,max}} = f_{\mathrm{exc}} \frac{d_{\mathrm{eff}}^2 F^2}{2C_p}$$

where, f_{exc} is the excitation frequency. Actual harvested power is lower and depends on electrical loading, extraction topology, rectification losses, mechanical-electrical coupling, and the fraction of stored energy recovered during each cycle.

This relation provides a simplified bridge between material physics and system-level performance. Domain alignment, domain-wall mobility, phase composition, and polarization stability influence d_{eff}, whereas dielectric permittivity, electrode area, and active-layer thickness determine C_p. Mechanical stiffness, packaging, mounting conditions, and strain-transfer efficiency determine the force or deformation delivered to the active material. Flexoelectric contributions may additionally modify the effective polarization response in structures subjected to strong strain gradients, particularly at small length scales.

These expressions are intended as design-level scaling relations rather than universal prediction equations. Under strain-driven or resonant excitation, displacement, stiffness, damping, resonance behavior, and electromechanical coupling must also be considered. Therefore, experimentally measured device-level harvested power should be used in autonomy conditions whenever available.

The dependence of electromechanical performance on polarization mechanisms explains why no single piezoelectric material simultaneously satisfies sensitivity, flexibility, stability, and integration requirements. Consequently, piezoelectric technology has progressed through successive material classes, each addressing limitations of earlier systems. The following section reviews this evolution and classifies modern piezoelectric materials according to their functional roles in autonomous sensing systems.

3. MATERIALS DEVELOPMENT AND CLASSIFICATION

The evolution of piezoelectric materials reflects a progressive shift from maximizing intrinsic electromechanical coefficients toward optimizing materials for system-level integration and energy-autonomous operation. Early research focused on demonstrating electromechanical coupling in crystalline materials, followed by maximizing output using engineered ceramics. Later developments prioritized mechanical compatibility through polymers and composites, while recent advances emphasize miniaturization and autonomous system integration. Figure 1 summarizes this transition, illustrating how the field evolved from material discovery toward functional IoT-oriented systems rather than purely improving intrinsic material properties.

Figure 1 emphasizes that material innovation has progressively aligned with application-driven constraints rather than purely crystallographic performance metrics.

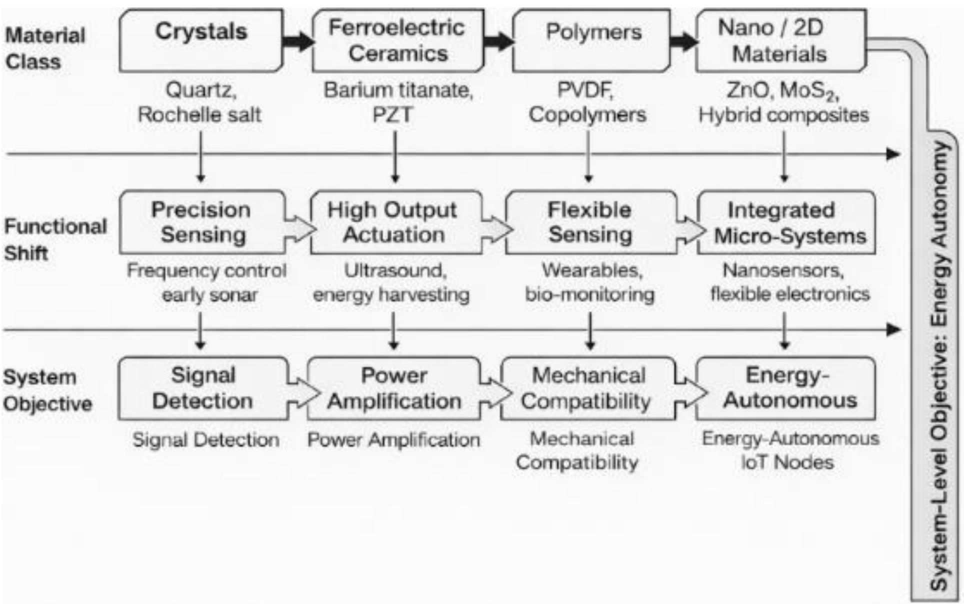

Figure 1. Timeline of piezoelectric material development and functional evolution

3.1 From intrinsic crystals to engineered ceramics

The earliest piezoelectric materials were naturally occurring crystals such as quartz, Rochelle salt, and tourmaline. These materials offered excellent chemical stability and reproducibility but produced relatively small electromechanical responses, restricting their use mainly to precision sensing and frequency-control applications.

The demand for stronger actuation and higher electrical output led to the development of ferroelectric ceramics. The discovery of barium titanate demonstrated that domain reorientation could significantly amplify polarization compared with intrinsic lattice distortion [31]. This development culminated in PZT, whose morphotropic phase boundary enables enhanced domain mobility and high electromechanical coupling [32]. Consequently, PZT became an industrial standard for actuators, ultrasonic transducers, and high-power electromechanical devices.

Subsequent advances introduced relaxor single crystals such as PMN-PT and PZN-PT, which exhibit exceptionally high piezoelectric coefficients suitable for medical imaging and precision-positioning systems [36]. However, their complex fabrication and lead content have motivated the development of environmentally safer alternatives. Lead-free materials, including potassium sodium niobate and modified barium titanate ceramics, have therefore been investigated through compositional engineering, phase-boundary control, and crystallographic texturing to approach the performance of lead-based systems [37, 38].

Recent KNN ceramics research increasingly focuses on multiscale phase engineering, crystallographic texturing, grain-orientation control, and defect regulation to enhance domain rotation and electromechanical response while retaining a lead-free composition [37]. Data-driven approaches have also been introduced to identify composition-structure descriptors associated with high d_{33} in KNN-based ceramics [39]. These developments indicate that the performance gap between lead-free and lead-based ceramics is increasingly being addressed through coordinated composition-microstructure design rather than composition modification alone.

Despite their high electromechanical performance, ceramic materials remain mechanically rigid and brittle, limiting their use in flexible electronics, wearable sensing, and systems subjected to repeated large deformation.

3.2 Polymeric piezoelectrics: Flexibility and conformability

The discovery of piezoelectricity in PVDF introduced mechanically compliant materials capable of conformable sensing [7]. In polymers, polarization originates primarily from aligned molecular dipoles rather than from conventional ceramic domain switching. Although this mechanism produces lower charge coefficients, the low dielectric permittivity of PVDF results in high voltage sensitivity. Polymer piezoelectrics are therefore particularly suitable for high-impedance sensing interfaces, wearable devices, and low-power IoT nodes.

Mechanical stretching and electrical poling promote formation of the polar β-phase responsible for the piezoelectric response [33]. Copolymers and electrospun nanofibers can further improve dipole alignment, electroactive-phase content, and mechanical flexibility [40].

Recent research has extended these approaches toward microstructure-engineered nanofibers, porous films, conductive composites, and mechanically compliant sensor architectures. These strategies aim to improve strain transfer, increase the electroactive β-phase fraction, and maintain sensitivity under repeated deformation [41]. Recent reviews of flexible piezoelectric sensors emphasize filler engineering, fabrication optimization, microstructure control, cycle life, and integration with wearable intelligent systems.

Such materials are increasingly used in wearable sensors, biomedical patches, physiological monitoring, and human-motion recognition. However, polymeric piezoelectrics generally provide lower charge generation and electromechanical coupling than high-performance ceramics. Applications requiring larger harvested power or stronger actuation therefore commonly employ composite or hybrid material strategies.

3.3 Composite and hybrid architectures for property co-optimization

Composite piezoelectrics combine ceramic inclusions with polymer matrices to simultaneously achieve flexibility and sensitivity. Connectivity models such as particulate (0-3), fiber-reinforced (1-3), and layered (2-2) structures allow tuning of stiffness, permittivity, and coupling efficiency [42].

Nanoscale fillers such as ZnO nanowires, carbon nanotubes, and graphene can enhance interfacial polarization, charge transport, and local stress transfer [43]. Additive-manufacturing and printing techniques further enable scalable fabrication of conformable devices, patterned sensors, and piezoelectric structures embedded directly within host components [44].

Recent composite designs increasingly exploit porous or fibrous architectures, multiscale filler networks, and controlled ceramic-polymer interfaces to improve electromechanical response without sacrificing flexibility. Their performance nevertheless depends strongly on filler dispersion, interface adhesion, dielectric contrast, percolation behavior, and the efficiency with which mechanical strain is transferred to the active phase [45-48].

3.4 Nanostructured and two-dimensional piezoelectrics

The demonstration of piezoelectricity in ZnO nanowires showed that electromechanical coupling persists at nanoscale dimensions, enabling nanogenerators capable of converting small mechanical deformations into electrical signals and energy [34]. ZnO nanowires are particularly attractive because they combine nanoscale dimensions, semiconductor functionality, and compatibility with flexible substrates.

Atomically thin materials such as monolayer MoS_2 were subsequently shown to exhibit intrinsic piezoelectricity because of broken inversion symmetry [49]. Their atomic thickness and mechanical flexibility make them promising for ultrathin sensors and flexible electronic platforms. However, the coefficients reported for two-dimensional materials are often defined per unit length or through effective device parameters and should not be interpreted as directly equivalent to bulk d_{33}.

Data-driven and high-throughput computational methods are increasingly being applied to nanoscale materials. Machine-learning models can assist in identifying relationships among composition, symmetry, bonding, electronic structure, and functional response, thereby reducing the number of candidates requiring full first-principles or experimental evaluation. However, screening results should be distinguished carefully according to whether the predicted property is piezoelectricity, mechanical flexibility, bandgap, or resistive behavior.

Hybrid nanosheet-polymer and nanowire–polymer structures can improve mechanical durability, strain transfer, and electrical output while retaining flexibility [45]. Such architectures are particularly useful when atomically thin or nanoscale active materials require a mechanically robust support, improved interfacial coupling, or protection from environmental degradation.

Nanostructured and two-dimensional materials therefore represent a transition from conventional actuator-dominated design toward multifunctional platforms optimized for miniaturization, flexibility, sensing, and integration with energy-constrained electronics.

3.5 Functional classification for autonomous systems

While Table 1 compares intrinsic electromechanical coefficients, practical material selection also depends on mechanical compliance, durability, operating mode, fabrication compatibility, and system-level energy requirements. Different applications may prioritize flexibility, voltage sensitivity, fatigue resistance, or output power rather than maximizing a single material coefficient. Table 2 therefore classifies representative piezoelectric materials according to their functional roles in autonomous sensing systems.

Table 2. Functional classification and representative electromechanical properties of piezoelectric materials for autonomous Internet of Things (IoT) systems

Material	Type	d_{33} (pC/N)	k_t	Flexibility	Dominant Advantage	Typical Role in IoT Systems
Lead zirconate titanate (PZT) [21, 31]	Ceramic	300–600	0.7	Low	High charge output, strong coupling	Actuators, ultrasonic transducers, high-power harvesters
$BaTiO_3$ [31, 38]	Ceramic	~190	0.5	Low	Stable ferroelectric response	Multilayer sensors, integrated ceramic devices
PVDF [7, 33]	Polymer	20–30	0.2	High	High voltage sensitivity, low permittivity	Wearables, microphones, flexible sensors
PVDF-PZT composite [42, 46, 48]	Hybrid	~150	0.4	Medium	Balanced charge and compliance	Biomedical patches, conformable monitoring systems
ZnO nanowire [34]	Nano	8-15	~0.35	High	Nanoscale integration, miniaturization	Nanogenerators, microsystems
MoS_2 monolayer [49]	2D	Reported using 2D/effective coefficients; not directly comparable with bulk d_{33}	–	High	Atomic thickness, flexible electronics integration	Flexible electronics, ultra-thin sensing platforms

Note: Values are representative of the cited literature and may vary with composition, dimensionality, processing, poling, measurement direction, substrate constraint, frequency, and characterization method. Values reported for nanoscale and two-dimensional materials should not be directly compared with bulk coefficients unless the coefficient definitions, normalization methods, and mechanical boundary conditions are equivalent. Polyvinylidene fluoride (PVDF).

Table 2 demonstrates that optimal material selection is application-driven rather than coefficient-driven. High-coupling ceramics such as PZT remain suitable for actuation and high-power harvesting, whereas polymers provide voltage sensitivity and mechanical compatibility for wearable and distributed sensing. Composite and nanoscale systems enable co-optimization of flexibility, miniaturization, and electromechanical response. Modern piezoelectric-material development is therefore increasingly guided by system integration, durability, and energy-autonomy requirements rather than by maximization of a single intrinsic coefficient.

4. FABRICATION AND CHARACTERIZATION OF PIEZOELECTRIC DEVICES

The practical performance of piezoelectric devices is governed not only by intrinsic material coefficients but by fabrication-induced factors that determine domain alignment, defect density, electrode interfaces, and mechanical boundary conditions. Because these parameters directly influence extractable electrical energy and long-term stability, processing strategy becomes a central determinant of energy-autonomous operation. Fabrication therefore plays a critical role in translating material properties into practical sensing and energy-harvesting performance. This section focuses on how processing strategies influence electromechanical behavior rather than providing an exhaustive description of manufacturing techniques.

4.1 Ceramic processing and domain engineering

Ferroelectric ceramics are typically fabricated using solid-state synthesis followed by high-temperature sintering to achieve dense polycrystalline structures. During sintering, grain growth and phase composition determine domain mobility and therefore piezoelectric response [50]. Post-processing electrical poling aligns ferroelectric domains, converting randomly oriented dipoles into a macroscopic polarization state.

Advanced processing techniques such as tape casting and multilayer lamination allow fabrication of stacked actuators and sensors with high electric field concentration at moderate voltages [47]. Grain texturing and compositional grading further enhance coupling coefficients by promoting domain alignment along preferred crystallographic orientations [51]. However, high-temperature processing may introduce residual stresses and microcracks that reduce long-term reliability under cyclic loading. Such microstructural defects increase dielectric loss and leakage current, reducing the effective energy that can be harvested under low-strain IoT conditions.

4.2 Polymer processing and flexible device fabrication

Polymeric piezoelectrics require alignment of molecular dipoles rather than crystal domains. This is typically achieved through mechanical stretching combined with electrical poling, which promotes formation of the electroactive β-phase in PVDF [33]. Electrospinning enables fabrication of nanofiber mats with highly aligned dipoles and improved sensitivity [52].

Flexible electrodes based on thin metals, conductive polymers, or carbon nanomaterials are deposited using sputtering, evaporation, or printing techniques. Encapsulation layers are commonly added to protect devices from humidity and mechanical fatigue. Because polymer devices operate at low stiffness, mechanical boundary conditions strongly influence the output signal, making packaging a critical design parameter rather than a secondary step. In flexible IoT platforms, packaging stiffness directly modifies strain transfer efficiency, thereby altering the effective electromechanical conversion factor.

4.3 Thin-film and microfabrication techniques

For miniaturized sensors and MEMS devices, thin-film deposition techniques such as sol-gel processing, sputtering, pulsed laser deposition, and chemical vapor deposition are widely used [53]. These methods enable integration with semiconductor electronics and allow fabrication of microscale resonators, pressure sensors, and acoustic transducers.

At reduced thickness, substrate clamping constrains in-plane strain, often reducing effective d_{33} and coupling factors compared with bulk values, which must be accounted for in microscale energy harvesting designs. Microfabrication therefore requires careful design of electrode geometry and release structures to restore mechanical compliance. Patterning techniques including photolithography and etching define device geometry and resonance frequency.

4.4 Nanogenerator and hybrid device assembly

Nanostructured piezoelectrics are typically grown using hydrothermal synthesis, vapor deposition, or template-assisted methods to produce aligned nanowires and nanosheets [34]. Device assembly often involves embedding nanostructures within polymer matrices to enhance durability and mechanical stability [54].

Because nanogenerators operate under low mechanical input, interface engineering becomes critical. Contact resistance, surface states, and Schottky barrier formation at electrodes significantly influence electrical output [48]. Consequently, electrical contacts and encapsulation layers frequently determine device performance more strongly than intrinsic material properties. In low-power harvesting scenarios, even small increases in contact resistance can reduce usable power below the threshold required for autonomous sensing.

4.5 Characterization techniques

Evaluating piezoelectric performance requires combining electrical and mechanical measurements across multiple scales. Macroscopic coefficients are measured using quasi-static loading or resonance methods [25], while dynamic response is evaluated through vibration testing and impedance analysis. Piezoresponse force microscopy enables nanoscale observation of polarization switching and local defects [26]. Multiphysics simulation frameworks combining electromechanical and structural modeling — for example, coupled COMSOL and ANSYS analyses — have similarly been used to design and characterize cantilever-based microscopy probes, illustrating the broader role of coupled simulation tools in piezoelectric device and instrumentation development [55].

For energy harvesting applications, practical characterization includes output voltage, power density, load matching, and stability under cyclic excitation rather than relying solely on material coefficients. For autonomous IoT nodes, reliability must be evaluated under realistic mechanical excitation spectra rather than idealized laboratory sinusoidal loading, as performance degradation directly impacts energy feasibility [56].

Fabrication defines the achievable device performance, but autonomous operation requires efficient conversion, storage, and use of the harvested electrical energy. The next section therefore examines power management circuits and system-level integration enabling piezoelectric devices to operate as self-powered sensing nodes.

5. ENERGY HARVESTING AND POWER MANAGEMENT FOR SELF-POWERED OPERATION

Although piezoelectric materials directly convert mechanical deformation into electrical charge, the generated signal is typically intermittent, high-impedance, and poorly matched to electronic loads. Without proper conditioning, most of the harvested energy is lost. Efficient energy extraction and management are therefore essential for enabling autonomous sensing systems. This section is limited to the electrical-energy pathway from transducer output to regulated and stored power, including rectification, extraction, storage, duty cycling, and the system-level autonomy condition. Embedded inference methods and model-design considerations are discussed separately in Section 6.

5.1 Electrical nature of piezoelectric output

A piezoelectric device behaves electrically as a current source in parallel with an internal capacitance. Mechanical excitation produces alternating charge, resulting in an AC voltage whose amplitude depends on load impedance and excitation frequency [21]. Because the output impedance is typically very high, directly powering electronics leads to severe energy loss. As a result, the effective power delivered to electronics is often orders of magnitude lower than the theoretical electromechanical conversion predicted by material coefficients.

Maximum power transfer occurs only when the electrical load is matched to the internal capacitive reactance, which varies with frequency. Consequently, practical harvesting circuits must adapt to changing mechanical conditions rather than relying on fixed resistive loads [57].

5.2 Rectification and energy extraction circuits

The simplest interface consists of a diode bridge rectifier followed by a storage capacitor. However, voltage drops across diodes significantly reduce efficiency for low-amplitude signals [58]. To overcome this limitation, synchronized switching techniques were developed to actively control charge transfer.

Synchronized Switch Harvesting on Inductor (SSHI) circuits invert the voltage across the piezoelectric element at displacement extrema, dramatically increasing extracted power [57, 59]. Synchronous Electric Charge Extraction (SECE) circuits transfer energy directly into storage elements, making them suitable for irregular mechanical excitations [60]. These techniques can improve harvested power several times compared with passive rectification. However, their implementation increases circuit complexity and standby consumption, which must be carefully balanced against net energy gain in low-power IoT deployments.

Recent approaches employ adaptive and nonlinear interfaces capable of tracking optimal extraction conditions under variable vibration environments [61].

5.3 Energy storage and power regulation

Because mechanical excitation is intermittent, harvested energy must be accumulated before use. Storage elements typically include capacitors for short-term buffering and rechargeable batteries or supercapacitors for long-term operation [62]. Power management integrated circuits regulate voltage and enable cold-start operation when initial energy levels are extremely low. The electro-thermal reliability of the semiconductor switches used within these power-management circuits has also been examined using coupled Multiphysics simulation approaches, providing insight into thermal limits relevant to compact IoT power stages [63].

Efficient regulation is critical since IoT electronics often require stable DC voltages while the harvester provides irregular pulses. Duty-cycled operation is therefore commonly used, where sensing and communication occur only after sufficient energy has been accumulated [41].

5.4 System-level power budget and operation modes

The feasibility of a self-powered sensor depends on the balance between harvested energy and total system consumption [9]. In many low-power IoT platforms, wireless transmission requires substantially more energy per event than sensing or local computation, although the exact ratio depends on the radio protocol, payload, transmission power, and hardware platform.

Modern self-powered nodes therefore commonly employ event-driven and duty-cycled operation. The system remains in a low-power state until sufficient energy has been accumulated or a relevant mechanical event is detected, after which sensing, processing, and communication are performed according to the available energy budget. Reducing the frequency and duration of radio activity is particularly important in communication-dominated systems because it can significantly lower average power demand.

Hybrid harvesters combining piezoelectric, triboelectric, and photovoltaic mechanisms can further stabilize the energy supply under variable environmental conditions [64]. The present section focuses on the energy-management and operating-mode implications of these architectures. The signal-processing and machine-learning methods used to determine which events or features should be transmitted are discussed separately in Section 6.

5.5 Energy budget for autonomous inference

The feasibility of self-powered intelligent sensing depends on whether the usable harvested electrical energy exceeds the total energy required for sensing, computation, and communication during an operational cycle. The net operational energy can be expressed by Eq. (3):

$$\eta_{\mathrm{PM}} E_{\mathrm{harv}} \geq E_{\mathrm{sense}} + E_{\mathrm{infer}} + E_{\mathrm{tx}} \tag{3}$$

where, E_{harv} is the electrical energy generated by the piezoelectric transducer before power-management losses, η_{PM} is the efficiency of the power-management interface, and E_{sense}, E_{infer}, and E_{tx} are the energies required for data acquisition, embedded inference, and wireless transmission, respectively. Eq. (3) applies to one completed operational cycle and assumes that sufficient stored energy is available to execute that cycle; it does not describe the preceding cold-start or energy-accumulation transient. This cycle-level formulation also does not explicitly include continuous leakage and standby losses, which are incorporated in the time-averaged autonomy condition presented in Eq. (4).

Table 3. Representative order-of-magnitude energy costs reported for low-power Internet of Things (IoT) operations

Operation or Loss Term	Typical Energy/Power Scale	Notes
Sensor sampling + analog-to-digital converter (ADC) [9, 65]	~0.1–10 μJ	System-level range including sensor and analog-front-end operation; ADC-only implementations may consume substantially less.
Lightweight inference (TinyML) [14, 66]	~1–100 μJ	Depends on model architecture, processing platform, quantization, and memory access.
BLE advertisement / short packet [67, 68]	~10–1000 μJ	Depends on payload, transmit power, radio startup, advertising channels, and protocol overhead.
Microcontroller unit (MCU) wakeup and housekeeping [9, 10]	~1–50 μJ	Depends on sleep mode and peripherals.
Storage and standby leakage [69]	Device- and time-dependent; reported as leakage current or power	May dominate during long idle periods; depends on storage technology, voltage, temperature, and conditioning.

Note: The listed values represent approximate orders of magnitude compiled from the cited literature. Sensor and ADC energy may include different portions of the analog front end; tiny machine learning (TinyML) energy depends on the benchmark task and processing platform; and bluetooth low energy (BLE) energy depends on whether wake-up, channel switching, protocol overhead, and retransmission are included. Storage leakage is a continuous loss and is therefore more appropriately expressed as leakage current or power than as energy per operation.

Table 3 summarizes representative order-of-magnitude energy costs for low-power IoT operations. These values are intended for preliminary energy budgeting rather than as universal limits because consumption varies considerably with hardware, firmware, measurement boundaries, payload size, and operating conditions.

Table 3 illustrates that wireless communication may remain the dominant energy term even when sensing and local computation are reduced to the microjoule range. The energy budget therefore favors architectures that reduce transmission frequency, radio-on time, and payload size. Improvements in power-management efficiency and reductions in storage or standby leakage may also produce substantial gains in the autonomy margin.

The detailed signal-processing and TinyML methods used to convert sensor waveforms into compact features, classifications, or event flags are discussed in Section 6. The present section is limited to quantifying the energy available for these operations and establishing the conditions under which they can be supported.

5.6 System-level autonomy condition

While previous sections discussed harvesting circuits and duty-cycled operation qualitatively, autonomous sensing ultimately depends on a simple quantitative requirement: the time-averaged usable harvested power must exceed the total average power required for sensing, computation, communication, and standby operation. This condition can be expressed as:

$$\eta_{\text{PM}} P_{\text{harv}} > f_s E_{\text{sense}} + f_i E_{\text{infer}} + f_t E_{\text{tx}} + P_{\text{leak}} \tag{4}$$

where, P_{harv} is the average electrical power available at the output of the piezoelectric transducer before power-management losses, η_{PM} is the efficiency of the power-management interface (commonly implemented as a power-management integrated circuit, PMIC), E_{sense}, E_{infer}, and E_{tx} represent the energy required for sampling, local inference, and wireless transmission, respectively, and f_s, f_i, and f_t denote the corresponding operation frequencies. P_{leak} accounts for storage, standby, and other time-averaged parasitic losses.

Eq. (4) is a time-averaged rather than an instantaneous power balance. It is evaluated over an averaging interval sufficiently long to contain representative sensing, inference, communication, and idle periods. The operation frequencies f_s, f_i, and f_t therefore represent average event rates over this interval. The formulation assumes statistically stationary or periodically repeatable excitation and operating conditions during the averaging period.

Frequency effects are included at the system level through the excitation-dependent value of P_{harv} and through the operation frequencies multiplying the energy cost of each task. However, Eq. (4) does not explicitly resolve waveform-level dynamics, rectifier transients, storage-voltage ripple, cold-start behavior, or the initial charging of an empty storage element. These transient conditions require a time-dependent circuit and storage model. Accordingly, satisfying Eq. (4) indicates long-term average energy feasibility but does not, by itself, guarantee successful startup or uninterrupted operation during short-term excitation deficits.

As discussed in Section 2.4, P_{harv} depends not only on the intrinsic piezoelectric response but also on dielectric permittivity, device capacitance, geometry, excitation frequency, mechanical loading, stiffness, damping, strain-transfer efficiency, and boundary conditions. The factor η_{PM} subsequently accounts for losses associated with rectification, energy extraction, regulation, and storage interfacing.

For design comparison, the inequality in Eq. (4) can be expressed through the dimensionless autonomy ratio $\mathcal{A}$ (Eq. (5)):

$$\mathcal{A} = \frac{P_{\text{usable}}}{P_{\text{demand}}} = \frac{\eta_{\text{PM}} P_{\text{harv}}}{E_{\text{sense}} f_s + E_{\text{infer}} f_i + E_{\text{tx}} f_t + P_{\text{leak}}} \tag{5}$$

where, $P_{\text{usable}} = \eta_{\text{PM}} P_{\text{harv}}$, and the denominator represents the total time-averaged power demand. A value of $\mathcal{A} < 1$ indicates an average energy deficit, $\mathcal{A} = 1$ represents the break-even condition, and $\mathcal{A} > 1$ indicates an average energy surplus under the stated operating conditions. This ratio does not replace detailed transducer or circuit models; rather, it provides a common metric for comparing interventions made at different design layers.

This relation highlights that system autonomy is not governed by material performance alone. Increasing the effective piezoelectric response can raise P_{harv} under appropriate mechanical and electrical conditions, but comparable or larger gains may be obtained by reducing the communication frequency f_t, lowering the inference energy E_{infer}, improving η_{PM}, or minimizing P_{leak}. In communication-dominated deployments, reducing wireless transmissions may improve the autonomy margin more strongly than a modest increase in a single intrinsic piezoelectric coefficient.

Eq. (5) therefore links the principal design layers as follows:

•Material and device design influence P_{harv}.
•Circuit architecture determines η_{PM}.
•Embedded intelligence determines E_{infer} and f_i.
•Communication strategy determines E_{tx} and f_t.
•Storage and standby behavior determines P_{leak}.

Consequently, achieving sustained autonomous operation requires co-optimization across these layers rather than maximization of a single performance metric. This framework explains why high-output laboratory harvesters may still fail to support practical deployments: improvements in intrinsic material coefficients alone may not compensate for inefficient communication, poor interface efficiency, or excessive standby and storage losses.

Eq. (5) therefore establishes the energy envelope within which embedded inference must operate, while Section 6 examines how the available computational and communication budgets can be used efficiently.

5.7 Illustrative cross-layer comparison

To demonstrate how the autonomy ratio introduced in Eq. (5) can be used as a design tool, an illustrative comparison is performed between a material-level intervention and a communication-level intervention. The purpose of this example is not to reproduce a specific experimental device, but to show how changes made at different system layers can be evaluated using the same autonomy criterion.

Representative energy values within the ranges reported in Table 3 are considered:

$$E_{\text{sense}} = 2\ \mu\text{J}, E_{\text{infer}} = 20\ \mu\text{J}, E_{\text{tx}} = 200\ \mu\text{J}$$

with storage and standby losses represented by

$$P_{\text{leak}} = 5\ \mu\text{W}$$

Sensing and local inference are assumed to occur at 1 Hz. A baseline piezoelectric device with $d_{33} = 300$ pC/N is assumed to provide 100 μW of usable average post-interface power under the specified mechanical excitation. At a wireless transmission frequency of 1 Hz, the corresponding average power demand is:

$$P_{\text{demand}} = E_{\text{sense}} f_s + E_{\text{infer}} f_i + E_{\text{tx}} f_t + P_{\text{leak}} = 227\ \mu\text{W}$$

Using Eq. (5), the baseline autonomy ratio is $\mathcal{A}_0 = \frac{100}{227} = 0.44$, indicating an average energy deficit.

Using the material-to-power scaling established in Section 2.4, a material-level intervention can be estimated for a force-driven piezoelectric element. Holding force, geometry, capacitance, excitation frequency, and interface efficiency constant, usable power scales approximately as in Eq. (6):

$$\frac{P_{\text{usable},2}}{P_{\text{usable},1}} \approx \left(\frac{d_{33,2}}{d_{33,1}}\right)^2 \quad (6)$$

This scaling relation assumes force, geometry, capacitance, excitation frequency, and interface efficiency remain constant, and is intended only as a first-order estimate within a single device design—it should not be used to compare different material systems or device architectures, since permittivity, capacitance, elastic compliance, electromechanical coupling, and interface losses can vary simultaneously across materials or geometries. Whenever device-level data are available, experimentally measured usable harvested power should be substituted directly into Eq. (5).

Increasing d_{33} from 300 to 500 pC/N therefore gives an idealized scaling factor of $\left(\frac{500}{300}\right)^2 \approx 2.78$.

Accordingly, the usable average power increases from 100 µW to approximately 278 µW. Since the operating frequencies and energy costs remain unchanged, the average demand remains 227 µW, giving $\mathcal{A}_{d_{33}} = \frac{278}{227} = 1.22$.

The material-level intervention therefore moves the node slightly above the break-even autonomy threshold.

A system-level intervention can instead retain the original $d_{33} = 300$ pC/N while reducing the wireless transmission frequency from 1 to 0.1 Hz. Sensing and local inference are maintained at 1 Hz, but only one out of every ten inference outcomes is transmitted. The resulting average demand becomes:

$$P_{\text{demand,event}} = (2)(1) + (20)(1) + (200)(0.1) + 5 = 47\ \mu\text{W}$$

With the usable harvested power remaining at 100 µW, the corresponding autonomy ratio becomes $\mathcal{A}_{\text{event}} = \frac{100}{47} = 2.13$.

Table 4 summarizes the resulting autonomy ratios and illustrates, under the selected operating conditions, how a material-level increase in piezoelectric response compares with a communication-level reduction in transmission frequency.

Table 4. Illustrative comparison of material-level and communication-level interventions using the autonomy ratio

Case	d_{33} (pC/N)	f_{tx} (Hz)	Usable Harvested Power (μW)	Average Demand (μW)	Autonomy Ratio $\mathcal{A}$	Operating Condition
Baseline	300	1.0	100	227	0.44	Energy deficit
Increased piezoelectric response	500	1.0	278	227	1.22	Small energy surplus
Event-driven transmission	300	0.1	100	47	2.13	Large energy surplus

Note: The material-level power scaling is an idealized force-driven sensitivity estimate assuming unchanged force transfer, device capacitance, geometry, excitation frequency, mechanical boundary conditions, and interface efficiency. It should not be interpreted as a universal comparison between different materials or device structures.

Under the selected conditions, both interventions move the sensing node above the break-even threshold. However, reducing the transmission frequency produces the larger autonomy margin because wireless communication is the dominant energy-consumption term in the assumed power budget. The material-level intervention increases usable harvested power by approximately 178%, whereas reducing the transmission frequency by 90% lowers the total average demand by approximately 79%.

This comparison is a controlled sensitivity analysis rather than a universal ranking of materials or design strategies. The approximate d_{33}^2 dependence applies only when the applied force, geometry, effective capacitance, excitation frequency, mechanical boundary conditions, and interface efficiency are held constant. When different materials or device structures are compared, dielectric permittivity, capacitance, elastic compliance, electromechanical coupling, dielectric loss, resonance behavior, strain-transfer efficiency, and interface losses may change simultaneously. Therefore, experimentally measured usable harvested power should be inserted into Eq. (5) whenever device-level data are available, rather than estimating system feasibility from d_{33} alone [21].

The example demonstrates the practical role of the cross-layer framework. Material improvements, interface optimization, inference reduction, communication duty cycling, and leakage mitigation can be compared using a common system-level metric. The dominant intervention depends on the application-specific energy budget: communication reduction is most effective in radio-dominated systems, whereas transducer and interface improvements become more important when mechanical input is weak, or communication is already infrequent.

5.8 Design-oriented architecture selection

The autonomy condition can be translated into practical design choices by identifying the term that dominates the energy budget in a given application. Rather than attempting to maximize all subsystem performance simultaneously, the design process should prioritize the principal material, circuit, computational, or communication constraint. Table 5 summarizes representative architecture choices for several operating scenarios. These recommendations are indicative rather than prescriptive and should be validated using application-specific excitation spectra, device measurements, and energy budgets.

Table 5 illustrates that architecture selection should be guided by the dominant energy constraint rather than by absolute material performance alone. In low-frequency, communication-dominated applications, reducing transmission activity may improve the autonomy margin more effectively than increasing a single piezoelectric coefficient. In continuously excited systems, stable energy extraction and impedance matching may become more important, whereas long-duration deployments may be limited primarily by material fatigue, interface degradation, and storage leakage. Engineering effort should therefore focus on the limiting term identified through Eq. (5), while recognizing that the preferred material, circuit, inference model, and communication protocol remain application-dependent.

Table 5. Representative architecture choices derived from the system-level autonomy condition

Application Scenario	Dominant Constraint	Candidate Material	Candidate Interface Circuit	Embedded Intelligence Strategy	Communication Strategy
Wearable or human-motion sensing	Low frequency and small strain	PVDF or polymer composite	SECE or low-loss active rectifier	Lightweight neural network or threshold detection	Event-driven BLE advertisement
Structural monitoring	Long-term reliability	PZT ceramic or robust composite	SSHI or resonant extraction	Spectral-feature classification	Periodic summary transmission
Machinery vibration monitoring	Continuous vibration	PZT or single crystal	Impedance-matched rectifier	Online anomaly detection	Edge aggregation before transmission
Sporadic excitation, such as doors or footsteps	Rare events	Hybrid piezoelectric–triboelectric system	Adaptive or maximum power point tracking (MPPT)-based interface	Wake-on-event inference	Transmit only detected events
Distributed large-scale IoT networks	Communication energy	Application-compatible stable material	High-efficiency power-management integrated circuit (PMIC)	Local event classification with gateway-level model aggregation	Cooperative edge gateway

Note: Polyvinylidene fluoride (PVDF), lead zirconate titanate (PZT), synchronous electric charge extraction (SECE), synchronized switch harvesting on inductor (SSHI), bluetooth low energy (BLE).

6. EDGE INTELLIGENCE AND MACHINE LEARNING INTEGRATION

Section 5 established the energy available for sensing, computation, and communication. The present section focuses on the information-processing layer: how piezoelectric signals are transformed into features or decisions using algorithms compatible with limited memory, computation, and intermittent power. Rather than revisiting harvesting circuits or the overall energy balance, the discussion addresses signal representation, TinyML models, local inference, robustness, and deployment constraints.

Mechanical energy captured by the transducer supports signal conditioning and local TinyML inference, while higher-level edge nodes aggregate information before optional cloud transmission. This architecture reduces radio activity by transmitting selected features or decisions rather than continuously streaming raw sensor data.

Traditional sensing architectures often transmit raw time-series data to an edge server or cloud platform. For energy-constrained piezoelectric nodes, local preprocessing and inference can reduce the amount and frequency of transmitted data. The benefit of edge intelligence therefore arises from converting high-volume sensor signals into sparse features, classifications, or alerts before transmission.

Figure 2 presents the hierarchical information-processing architecture considered in this section, showing how piezoelectric sensing, local inference, edge aggregation, and optional cloud communication are organized within an energy-constrained IoT system.

In Figure 2, the piezoelectric sensor converts mechanical inputs such as pressure, vibration, or strain into electrical signals, while the associated harvesting pathway supplies electrical energy to the sensing node. Local edge machine learning (edge ML) modules process the sensor output to detect events, extract features, or perform classification before communication. A higher-level edge layer may aggregate results from multiple nodes, while the IoT cloud is reserved for selected data storage, large-scale analysis, visualization, and model updates. This hierarchy reduces continuous raw-data transmission and supports energy-aware operation.

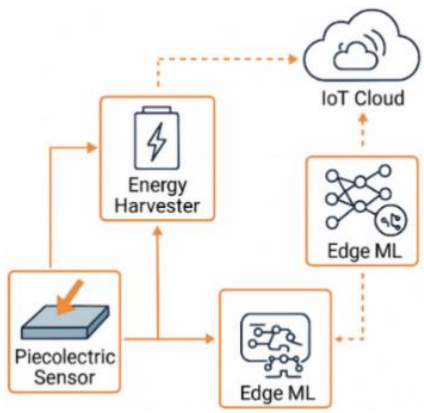

Figure 2. Hierarchical Internet of Things (IoT)-machine learning (ML) architecture for self-powered piezoelectric sensing

6.1 Signal characteristics and feature extraction

Piezoelectric sensors generate rich temporal signals containing information about vibration frequency, amplitude, and waveform shape. Instead of transmitting full time-series data, local preprocessing extracts relevant features such as peak amplitude, spectral components, or statistical descriptors. Feature reduction significantly lowers communication requirements and improves energy efficiency. Because energy consumption scales approximately with transmitted payload size and radio-on time, dimensionality reduction directly translates into extended operational lifetime.

In many applications, the signal itself provides sufficient power to trigger processing. The sensing event therefore acts simultaneously as both information source and energy source, enabling event-driven operation where computation occurs only when meaningful activity is detected [70].

6.2 Tiny machine learning and embedded machine learning

Recent advances in microcontroller architectures allow machine-learning inference to operate at microwatt power levels. TinyML algorithms compress neural networks and decision models to fit within limited memory and computational resources while maintaining acceptable accuracy [14, 71]. This simulation-to-classifier workflow—where a physics-based multiphysics model is used to generate training data for a lightweight machine-learning classifier that then performs real-time decision-making—has been demonstrated for non-piezoelectric optical sensing as a proof-of-concept design methodology and is conceptually transferable to embedded classification tasks in piezoelectric IoT nodes where experimental training data may be limited [72]. A related implementation of this approach applied to fuel-quality assessment reported that the resulting sensor design was compatible with low-cost, equipment-free, on-site testing—a positioning consistent with the deployment constraints emphasized throughout this review for autonomous IoT sensing nodes [73]. However, model compression must be balanced against classification robustness, particularly under varying mechanical excitation patterns typical of real deployments.

Common models include decision trees, support vector machines, and lightweight neural networks optimized through quantization and pruning techniques. These algorithms enable real-time classification tasks such as structural fault detection, activity recognition, and acoustic event identification directly on the sensor node.

Compared with cloud-based analysis, edge inference dramatically reduces communication energy consumption and latency, allowing sensors to respond immediately to detected events.

6.3 Self-powered intelligent sensing nodes

By combining energy harvesting with local inference, piezoelectric devices may operate as energy-autonomous sensing nodes under suitable excitation and duty-cycle conditions. A typical architecture consists of four stages:

•Mechanical stimulus generates electrical energy.
•Energy harvesting circuit stores sufficient charge.
•Microcontroller wakes from sleep mode.
•Embedded model classifies event and transmits only results.

Because transmission occurs only after classification, the energy budget shifts from communication-dominated to computation-dominated regimes only when transmission frequency is significantly reduced, enabling long-term operation under low mechanical excitation.

Such systems have been demonstrated for infrastructure monitoring, wearable health sensing, and human–machine interaction, where sensors detect specific events instead of continuously streaming raw data [71].

6.4 Challenges in learning from energy-constrained sensors

Despite promising results, several challenges remain. Limited memory restricts model complexity, making generalization difficult under variable environmental conditions. Training data must account for changes in mechanical excitation, temperature, and mounting conditions to avoid misclassification.

Additionally, intermittent power supply introduces non-volatile memory requirements and necessitates checkpointing strategies to preserve computation state during power loss [71]. Co-design of hardware, algorithms, and sensing materials is therefore essential to achieve reliable intelligent operation.

The convergence of materials engineering, energy harvesting electronics, and embedded intelligence enables autonomous sensing, yet practical deployment requires reliability, sustainability, and standardization. The next section discusses remaining limitations and emerging research directions shaping the future of piezoelectric IoT systems.

6.5 Design guidelines for deployable self-powered piezoelectric Artificial Intelligence of Things nodes

Based on the autonomy framework derived in Section 5, the following engineering principles can guide practical deployment:

•(G1) Material-readout alignment.

Select materials according to sensing impedance and functional role: high-voltage polymers for high-impedance sensing; high-coupling ceramics for actuation or high-force transduction.

•(G2) Capacitance–interface co-design.

Match device capacitance and electrode geometry to the chosen harvesting topology (rectifier, SSHI, SECE, maximum power point tracking (MPPT). Minimizing parasitic capacitance and leakage often yields greater gains than marginal increases in d_{33}.

•(G3) Packaging as functional component.

Mechanical boundary conditions determine effective strain transfer and long-term stability; validation must be performed under realistic mounting conditions.

•(G4) Explicit energy feasibility check.

Require $E_{\text{harv}}\eta_{\text{PMIC}}$ to exceed worst-case operational demand. Duty cycles should be derived from measured excitation statistics, not idealized sinusoidal laboratory tests.

•(G5) Local inference preference.

Convert waveforms into decisions using TinyML and transmit only sparse outputs; this strategy typically provides the largest net energy reduction.

•(G6) Robustness over peak accuracy.

Account for temperature drift, mounting variability, and aging in datasets; prioritize stable feature sets.

•(G7) Reproducible benchmarking.

Report excitation spectrum, impedance matching, storage leakage, and inference power to enable fair comparison.

7. CHALLENGES AND FUTURE PERSPECTIVES

Despite rapid advances, long-term maintenance-free systems remain rare in real-world deployment.

The convergence of advanced piezoelectric materials, low-power electronics, and embedded machine learning has enabled the emergence of autonomous sensing nodes. However, large-scale deployment of self-powered intelligent IoT systems remains limited by interdisciplinary challenges spanning materials science, device engineering, circuit design, and data processing. Addressing these challenges requires coordinated optimization across all system layers rather than isolated improvements in individual components.

A recurring gap across the literature is the mismatch between laboratory demonstrations and field deployment constraints. Many prototypes report high peak voltages or power densities under controlled excitation yet omit long-duration fatigue, storage leakage, and realistic mounting variability—factors that can reduce net usable energy by orders of magnitude. Similarly, ML-enabled sensing studies often report accuracy without reporting inference energy, memory footprint, or performance drift under changing boundary conditions. Addressing these reporting gaps is essential for translating piezoelectric Artificial Intelligence of Things (AIoT) concepts into scalable and maintainable sensor networks.

7.1 Materials and mechanical reliability

Although high-performance ceramics provide strong electromechanical coupling, their brittleness limits durability under repeated deformation and impact loading. Flexible polymers improve mechanical compliance but may exhibit lower charge sensitivity, polarization relaxation, and temperature-dependent degradation. In composite and flexible devices, interface delamination, electrode cracking, changes in contact resistance, and inefficient strain transfer may degrade performance even when the intrinsic piezoelectric phase remains functional [17, 29, 41].

Reliability results must be interpreted according to the applied loading mode. Electrical fatigue refers to degradation during repeated electric-field cycling and is commonly quantified through changes in remanent polarization, dielectric response, strain, or piezoelectric coefficients. Mechanical fatigue concerns cyclic stress, strain, bending, vibration, or impact and may lead to cracking, depolarization, or delamination. Device-level durability testing additionally includes electrodes, bonding layers, substrates, encapsulation, and electrical interconnections. Consequently, cycle counts obtained under different loading modes should not be treated as directly equivalent lifetime measures.

Table 6. Representative fatigue and durability results reported for piezoelectric materials and devices

Material or Device Class	Loading Mode	Representative Reported Cycling	Reported Observation	Implication for Autonomous Internet of Things (IoT) Deployment
Bulk PZT ceramic [29, 74]	Bipolar electrical-field cycling	Up to 10^6 cycles	Polarization, dielectric, strain, and piezoelectric degradation depend on cycling temperature and domain-switching behavior	Electrical switching endurance cannot be inferred from mechanical vibration tests
Soft PZT ceramic [75]	Bipolar electrical cycling under controlled mechanical and thermal conditions	Surface cracking observed after approximately 3.6×10^5 cycles under the reported conditions	Fatigue was associated particularly with domain switching near the coercive field, defect redistribution, charge injection, and crack initiation	High-field devices require application-specific electrical and mechanical fatigue limits
PVDF-TrFE nanofiber composite [76]	Compressive mechanical fatigue	10^6 cycles	Mechanical and electrical properties, including sensing response, were maintained after the reported test	Selected polymer-composite devices can exceed short proof-of-concept validation, although electrode and mounting reliability remain important
Flexible metal/interconnect system [17]	Repeated bending	Test-specific number of cycles and bending radius	Resistance change and interfacial damage depend on conductor architecture and deformation conditions	Electrode or interconnect failure may occur before intrinsic degradation of the piezoelectric layer
ZnO nanogenerators [77]	Repeated mechanical excitation	Commonly $10^3 – 10^5$ cycles in representative demonstrations	Stable output may be maintained over the tested interval, but protocols vary considerably among devices	Short cycling demonstrations confirm repeatability but do not establish multi-year reliability
Flexible piezoelectric sensors and composites [41]	Bending, stretching, compression, or repeated human-motion loading	Device-dependent, often $10^3 − 10^6$ cycles	Performance depends on active material, electrode flexibility, interface adhesion, encapsulation, and loading amplitude	Reliability assessment must include the entire device stack and environmental exposure

Note: Polyvinylidene fluoride (PVDF), lead zirconate titanate (PZT).

Table 6 summarizes representative fatigue and durability results across major piezoelectric material and device classes. The reported values are illustrative rather than universal because loading amplitude, cycling frequency, temperature, geometry, mounting conditions, electrode design, and failure criteria vary considerably among studies.

Table 6 shows that reported durability spans several orders of magnitude and cannot be interpreted independently of loading mode. Bulk PZT studies report electrical cycling up to approximately 10^6 cycles, while selected polymer-composite systems have maintained sensing performance after 10^6 mechanical cycles. By contrast, many nanogenerator demonstrations remain limited to shorter cycling intervals. Flexible devices may additionally fail through electrode cracking, interfacial delamination, or contact-resistance drift before substantial degradation of the active piezoelectric phase occurs [17, 29, 41, 74-77].

The severity of the validation gap can be illustrated by converting laboratory cycle counts into equivalent continuous operating time. A device excited continuously at 1 Hz experiences approximately 3.15×10^7 cycles per year, whereas operation at 10 Hz corresponds to approximately 3.15×10^8 cycles per year. Accordingly, 10^5 cycles represent only approximately 27.8 h at 1 Hz and 2.78 h at 10 Hz. A 10^6-cycle test corresponds to approximately 11.6 days at 1Hz and 1.16 days at 10 Hz. Therefore, even apparently extensive laboratory tests may cover only a small fraction of the accumulated loading expected in continuously vibrating machinery or infrastructure applications.

The implications differ for event-driven wearables and sporadically activated sensors, for which the accumulated number of cycles may be considerably lower. Nevertheless, flexible devices introduce additional degradation mechanisms associated with bending radius, interfacial shear, electrode cracking, sweat and humidity exposure, temperature variation, washing, and packaging [17, 41]. In such systems, electrode and interface failure may dominate before a measurable loss of intrinsic piezoelectric polarization occurs.

A meaningful reliability assessment for autonomous piezoelectric IoT devices should therefore report the loading waveform and amplitude, cycling frequency, total cycle count, temperature, humidity, mounting and packaging conditions, electrode architecture, electrical load, and the criterion used to define failure. Output voltage alone is insufficient because it depends strongly on measurement impedance and device capacitance. Where applicable, studies should also report charge, power under a fixed electrical load, capacitance, leakage current, polarization or d_{33}, and contact resistance before and after cycling.

Recent materials development increasingly targets not only peak d_{33}, but also fatigue resistance, thermal and humidity stability, electrode-material interface integrity, and polarization retention under realistic cyclic loading. Future work should combine mechanically compatible electrodes, improved ceramic-polymer adhesion, robust encapsulation, accelerated aging, and multiphysics lifetime modeling. Such validation is necessary before short laboratory demonstrations can be extrapolated to deployment-relevant service periods.

7.2 Energy density and power stability

Ambient mechanical energy is inherently irregular and application-dependent. Even with efficient power-management circuits, insufficient excitation may interrupt sensing or computation. Hybrid harvesting approaches combining piezoelectric, triboelectric, and photovoltaic mechanisms offer a promising pathway to stabilize energy availability across varying environments. Another challenge lies in cold-start operation, where the system must accumulate enough energy to initiate computation. In low-frequency or sporadic excitation environments, the time-averaged harvested power may fall below the standby leakage power of storage elements, leading to a net energy deficit. Ultra-low-leakage storage elements and adaptive duty-cycling strategies will be required for reliable operation under weak mechanical inputs. Long-term deployments of vibration-powered sensor nodes show that harvested energy strongly depends on environmental variability and mounting conditions, reinforcing the need for adaptive harvesting strategies and hybrid energy management approaches [74, 75].

7.3 Energy-aware embedded intelligence

Machine-learning algorithms designed for conventional embedded systems often assume stable power supply and memory availability. In energy-harvesting devices, intermittent power may interrupt processing, requiring non-volatile memory and checkpointing strategies. Model compression, quantization, and event-driven inference must therefore be co-designed with sensing hardware.

Recent demonstrations of ultra-low-power inference hardware and energy-adaptive neural network architectures further confirm that embedded intelligence can operate within harvested energy budgets. Future TinyML frameworks may incorporate adaptive inference, where model complexity dynamically adjusts to available energy. Neuromorphic and spiking neural networks also offer potential for extremely low-power processing compatible with harvested energy levels.

7.4 System integration and standardization

Currently, piezoelectric IoT research lacks standardized datasets and performance metrics. Reported power density, sensitivity, and accuracy values are often measured under incomparable conditions, making fair evaluation difficult. Establishing benchmark excitation profiles and unified reporting protocols would significantly accelerate technological maturity. Reporting should include excitation spectrum, mechanical boundary conditions, load matching, inference energy per decision, and storage leakage over time. Recent efforts toward shared datasets and benchmarking methodologies for self-powered sensing and edge intelligence aim to improve reproducibility and fair comparison across reported systems [78, 79].

Integration with wireless protocols and edge computing architectures also remains challenging. Reliable large-scale deployment requires interoperability between sensing nodes, edge processors, and cloud analytics while maintaining strict energy budgets.

7.5 Sustainable manufacturing and future outlook

Environmental considerations increasingly influence material selection and device fabrication. Environmental impact must be evaluated not only at the material level but across the lifecycle, including encapsulation polymers, electronics disposal, and recyclability of composite architectures [80]. Lead-free piezoelectric ceramics, recyclable substrates, and low-temperature processing methods will be essential for sustainable mass production [81]. Emerging research also highlights recyclable substrates, environmentally friendly processing, and scalable printed electronics as key elements for sustainable large-scale deployment [82].

Looking forward, further progress in piezoelectric IoT systems will likely depend on the coordinated development of smart materials, adaptive power management, and embedded intelligence. As these layers mature, sensors are expected to move beyond passive measurement toward greater on-node data interpretation and decision support, provided that reliability, benchmarking, and system-level validation keep pace. Achieving this requires holistic design approaches in which materials, electronics, and algorithms are optimized jointly rather than independently.

The developments discussed above demonstrate that piezoelectric sensing is transitioning from component-level functionality to system-level autonomy. The following section summarizes the key contributions of this review and outlines its implications for future research.

8. CONCLUSIONS

This review examined the development of piezoelectric technology from fundamental electromechanical materials to self-powered sensing systems with embedded information processing. The discussion showed that material performance cannot be evaluated through a single piezoelectric coefficient. Polarization mechanisms, dielectric properties, mechanical compliance, device capacitance, fabrication, packaging, and boundary conditions jointly determine the electrical response available at the device level.

The analysis further showed that high intrinsic piezoelectric response does not necessarily translate into usable system power. Rectification, extraction efficiency, storage leakage, impedance matching, and duty cycling determine how much of the generated electrical energy becomes available to sensing, computation, and communication. The system-level autonomy condition introduced in this review is therefore presented as a design-oriented application of established energy-balance principles rather than as a new physical law.

The illustrative comparison demonstrated how material-level and architecture-level interventions can be evaluated using a common autonomy ratio. Under the selected assumptions, increasing d_{33} from 300 to 500 pC/N raised the estimated usable harvested power by a factor of approximately 2.78, whereas reducing transmission frequency from 1 to 0.1 Hz produced the larger autonomy margin because communication dominated the assumed power budget. This result is application-dependent and should not be generalized without measured excitation, transducer, circuit, and operational data.

Local feature extraction and TinyML inference can reduce communication demand by transmitting classifications, event flags, or compact features rather than continuously streaming raw sensor data. Their practical benefit nevertheless depends on inference energy, memory requirements, robustness to changing excitation and mounting conditions, and reliable operation under intermittent power.

Current evidence supports the feasibility of self-powered piezoelectric sensing in selected low-power and event-driven applications. However, widespread deployment remains limited by irregular mechanical excitation, storage and standby losses, interface degradation, material fatigue, inconsistent test conditions, and incomplete reporting of inference and communication energy. Progress will therefore require application-specific co-design, standardized characterization, and long-duration validation under realistic environmental and mechanical conditions.

Overall, piezoelectric autonomous sensing is best treated as a coupled materials-device-circuit-algorithm design problem. The framework presented in this review provides a structured basis for comparing these design layers, while final feasibility should be established using experimentally measured device power, system energy consumption, reliability data, and application-specific duty cycles.

REFERENCES

[1] Curie, J., Curie, P. (1880). Development by compression of polar electricity in hemihedral crystals with inclined faces [in French]. Bulletin of Mineralogy, 3-4: 90-93. https://doi.org/10.3406/bulmi.1880.1564

[2] Lippmann, G. (1875). Relations entre les phénomènes électriques et capillaires. Annales de chimie et de physique, 5(11): 494-549. http://electr003.chem.msu.ru/portret/electrocapillarity/Lippmann/1875_5_5.pdf.

[3] Duck, F.A. (2022). Paul Langevin, U-boats, and ultrasonics. Physics Today, 75(11): 42-48. https://doi.org/10.1063/PT.3.5122

[4] Ballato, A. (1995). Piezoelectricity: Old effect, new thrusts. IEEE Transactions on Ultrasonics, Ferroelectrics, and Frequency Control, 42(5): 916-926. https://doi.org/10.1109/58.464826

[5] Oppermann, R.H. (1947). Piezoelectricity: An introduction to the theory and applications of electromechanical phenomena in Crystals: By Walter Guyton Cady. 806 pages, drawings, 15 × 23 cms. New York, McGraw-Hill Book Company, Inc., 1946. Journal of the Franklin Institute, 244(2): 162-163. https://doi.org/10.1016/0016-0032(47)90068-9

[6] Uchino, K. (2010). Advanced Piezoelectric Materials: Science and Technology. Woodhead Publishing, pp. 1-678. https://doi.org/10.1533/9781845699758

[7] Kawai, H. (1969). The piezoelectricity of poly (vinylidene fluoride). Japanese Journal of Applied Physics, 8(7). https://doi.org/10.1143/jjap.8.975

[8] Pandey, R., Gangadhar, S.B., Grover, S., et al. (2019). Microscopic origin of piezoelectricity in Lead-Free Halide Perovskite: Application in nanogenerator design. ACS Energy Letters, 4(5): 1004-1011. https://doi.org/10.1021/acsenergylett.9b00323

[9] Roundy, S., Wright, P.K., Rabaey, J. (2003). A study of low level vibrations as a power source for wireless sensor nodes. Computer Communications, 26(11): 1131-1144. https://doi.org/10.1016/S0140-3664(02)00248-7

[10] Paradiso, J.A., Starner, T. (2005). Energy scavenging for mobile and wireless electronics. IEEE Pervasive Computing, 4(1): 18-27. https://doi.org/10.1109/MPRV.2005.9

[11] Man, D., Xu, G., Xu, H., Xu, D. (2022). Parametric analysis of nonlinear bi-stable piezoelectric energy harvester based on multi-scale method. Power Engineering and Engineering Thermophysics, 1(1): 19-32. https://doi.org/10.56578/peet010104

[12] Balizadeh, A.M., Yaghootian, A., Sedighi, H.M. (2026). Elastic wave isolation and highly directive wave propagation in architected two-dimensional metamaterials: An accelerated algebraic approach. Journal of Complex and Multiphysics Engineering Systems, 1(1): 1-37. https://doi.org/10.56578/jcmes010101

[13] Dagdeviren, C., Yang, B.D., Su, Y., et al. (2014). Conformal piezoelectric energy harvesting and storage from motions of the heart, lung, and diaphragm. Proceedings of the National Academy of Sciences of the United States of America, 111(5): 1927-1932. https://doi.org/10.1073/pnas.1317233111
[14] Warden, P., Situnayake, D. (2020). TinyML: Machine Learning with TensorFlow Lite on Arduino and ultra-Low-Power Microcontrollers (1st Edition). O'Reilly Media.
[15] Vrtagic, S., Hoxha, M., Abdelgalil, A., et al. (2025). Design and evaluation of a piezoelectric pressure sensor for mass detection with COMSOL and machine learning modeling. Measurement, 254: 117945. https://doi.org/10.1016/J.MEASUREMENT.2025.117945
[16] Mourched, B., Hoxha, M., Abdelgalil, A., et al. (2022). Piezoelectric-based sensor concept and design with machine learning-enabled using COMSOL Multiphysics. Applied Sciences (Switzerland), 12(19): 9798. https://doi.org/10.3390/app12199798
[17] Hwang, B., Han, Y., Matteini, P. (2022). Bending fatigue behavior of ag nanowire/cu thin-film hybrid interconnects for wearable electronics. Facta Universitatis, Series: Mechanical Engineering, 20(3): 553. https://doi.org/10.22190/FUME220730040H
[18] Dipon, W., Gamboa, B., Estrada, M., Flynn, W.P., Guo, R., Bhalla, A. (2023). Self-sustainable IoT-based remote sensing powered by energy harvesting using stacked piezoelectric transducer and thermoelectric generator. Micromachines, 14(7): 1428. https://doi.org/10.3390/mi14071428
[19] Rigo, F., Migliorini, M., Pozzebon, A. (2024). Piezoelectric sensors as energy harvesters for ultra low-power IoT applications. Sensors, 24(8): 2587. https://doi.org/10.3390/s24082587
[20] Voigt, W. (1910). Lehrbuch der Kristallphysik (mit Ausschluss der Kristalloptik). B.G. Teubner.
[21] Erturk, A., Inman, D.J. (2011). Effects of material constants and mechanical damping on power generation. In Piezoelectric Energy Harvesting, pp. 301-324. https://doi.org/10.1002/9781119991151.ch10
[22] Uchino, K. (1997). Piezoelectric Actuators and Ultrasonic Motors. Springer New York, NY.
[23] Priya, S., Inman, D.J. (2009). Energy Harvesting Technologies. Springer New York, NY. https://doi.org/10.1007/978-0-387-76464-1
[24] Schultheiß, J., Picht, G., Wang, J., et al. (2023). Ferroelectric polycrystals: Structural and microstructural levers for property-engineering via domain-wall dynamics. Progress in Materials Science, 136: 101101. https://doi.org/10.1016/j.pmatsci.2023.101101
[25] BerlinCourt, D.A., Curran, D.R., Jaffe, H. (1964). 3-piezoelectric and piezomagnetic materials and their function in transducers. Physical Acoustics, 169-270. https://doi.org/10.1016/b978-1-4832-2857-0.50009-5
[26] Kalinin, S.V., Bonnell, D.A. (2002). Imaging mechanism of piezoresponse force microscopy of ferroelectric surfaces. Physical Review B, 65(12): 125408. https://doi.org/10.1103/PhysRevB.65.125408
[27] Cohen, R.E. (1993). Origin of ferroelectricity in perovskites: The principal problems from a theoretical perspective. Ferroelectrics, 150(1). https://doi.org/10.1080/00150199308008689
[28] Tagantsev, A.K., Cross, L.E., Fousek, J. (2010). Domains in Ferroic Crystals and Thin Films. Springer New York, NY. https://doi.org/10.1007/978-1-4419-1417-0
[29] Genenko, Y.A., Glaum, J., Hoffmann, M.J., Albe, K. (2015). Mechanisms of aging and fatigue in ferroelectrics. Materials Science and Engineering: B, 192: 52-82. https://doi.org/10.1016/j.mseb.2014.10.003
[30] Wang, B., Gu, Y.J, Zhang, S.J, Chen, L.Q. (2019). Flexoelectricity in solids: Progress, challenges, and perspectives. Progress in Materials Science, 106: 100570. https://doi.org/10.1016/j.pmatsci.2019.05.003
[31] Jaffe, H. (1958). Piezoelectric ceramics. Journal of the American Ceramic Society, 41(11): 494-498. https://doi.org/10.1111/j.1151-2916.1958.tb12903.x
[32] Noheda, B., Cox, D.E., Shirane, G., Gonzalo, J.A., Cross, L.E., Park, S.E. (1999). A monoclinic ferroelectric phase in the $Pb(Zr_{1-x}Ti_x)O_3$ solid solution. Applied Physics Letters, 74(14): 2059-2061. https://doi.org/10.1063/1.123756
[33] Martins, P., Lopes, A.C., Lanceros-Mendez, S. (2014). Electroactive phases of poly(vinylidene fluoride): Determination, processing and applications. Progress in Polymer Science, 39: 683-706. https://doi.org/10.1016/j.progpolymsci.2013.07.006
[34] Wang, Z.L., Song, J.H. (2006). Piezoelectric nanogenerators based on zinc oxide nanowire arrays. Science, 312(5771): 242-246. https://doi.org/10.1126/science.1124005
[35] Sezer, N., Koç, M. (2021). A comprehensive review on the state-of-the-art of piezoelectric energy harvesting. Nano Energy, 80: 105567. https://doi.org/10.1016/j.nanoen.2020.105567
[36] Zhang, S., Shrout, T.R. (2010). Relaxor-PT single crystals: Observations and developments. IEEE Transactions on Ultrasonics, Ferroelectrics, and Frequency Control, 57(10): 2138-2146. https://doi.org/10.1109/TUFFC.2010.1670
[37] Lee, G.S., Kim, J.S., Kim, S.H., et al. (2024). Recent developments in (K, Na)NbO3-based lead-free piezoceramics. Micromachines, 15(3): 325. https://doi.org/10.3390/mi15030325
[38] Rödel, J., Jo, W., Seifert, K.T.P., Anton, E.M., Granzow, T., Damjanovic, D. (2009). Perspective on the development of lead-free piezoceramics. Journal of the American Ceramic Society, 92(6): 1153-1177. https://doi.org/10.1111/j.1551-2916.2009.03061.x
[39] Ma, B.W., Wu, X., Zhao, C.L., et al. (2023). An interpretable machine learning strategy for pursuing high piezoelectric coefficients in (K0.5Na0.5)NbO3-based ceramics. NPJ Computational Materials, 9(1): 229. https://doi.org/10.1038/s41524-023-01187-1
[40] Enuka, A., Keblawi, M., Sedar, E., Beachley, V. (2025). A continuous manufacturing approach for aligned PVDF nanofiber yarns with enhanced mechanical and piezoelectric properties. ACS Applied Polymer Materials, 7(9): 5429-5436. https://doi.org/10.1021/acsapm.5c00069
[41] Chen, Y.Y., Zhang, X.H., Lu, C. (2024). Flexible piezoelectric materials and strain sensors for wearable electronics and artificial intelligence applications. Chemical Science, 15(40): 16436-16466. https://doi.org/10.1039/d4sc05166a
[42] Newnham, R.E., Skinner, D.P., Cross, L.E. (1978).

Connectivity and piezoelectric-pyroelectric composites. Materials Research Bulletin, 13(5): 525-536. https://doi.org/10.1016/0025-5408(78)90161-7
[43] Pratihar, S., Patra, A., Sasmal, A., Medda, S.K., Sen, S. (2021). Enhanced dielectric, ferroelectric, energy storage and mechanical energy harvesting performance of ZnO-PVDF composites induced by MWCNTs as an additive third phase. Soft Matter, 17(37): 8483-8495. https://doi.org/10.1039/d1sm00854d
[44] Yi, H., Guo, X.Q., Chang, F.L., Cao, H.J., An, J., Chua, C.K. (2025). Ink-jetting-based conformal additive manufacturing: Advantages, opportunities, and challenges. International Journal of Extreme Manufacturing, 7(3): 032002. https://doi.org/10.1088/2631-7990/ada8e6
[45] Singh, V., Singh, B. (2023). MoS2-PVDF/PDMS based flexible hybrid piezo-triboelectric nanogenerator for harvesting mechanical energy. Journal of Alloys and Compounds, 941: 168850. https://doi.org/10.1016/j.jallcom.2023.168850
[46] Chen, J.X., Li, J.W., Cheng, C.C., Chiu, C.W. (2022). Piezoelectric property enhancement of PZT/Poly(vinylidenefluoride-co-trifluoroethylene) hybrid films for flexible piezoelectric energy harvesters. ACS Omega, 7(1): 793-803. https://doi.org/10.1021/acsomega.1c05451
[47] Zhang, J., Wang, X., Chen, X., Xia, X., Weng, G.J. (2022). Piezoelectricity enhancement in graphene/polyvinylidene fluoride composites due to graphene-induced $\alpha \rightarrow \beta$ crystal phase transition. Energy Conversion and Management, 269: 116121. https://doi.org/10.1016/j.enconman.2022.116121
[48] Suprapto, Eswanto, Jubaidah, et al. (2024). Multilayer PZT/PVDF composite films for high-performance force sensor and energy harvesting applications. Journal of Physics: Conference Series, 2908(1): 012029. https://doi.org/10.1088/1742-6596/2908/1/012029
[49] Wu, W.Z., Wang, L., Li, Y.L., et al. (2014). Piezoelectricity of single-atomic-layer MoS2 for energy conversion and piezotronics. Nature, 514(7523): 470-474. https://doi.org/10.1038/nature13792
[50] Malič, B., Koruza, J., Hreščak, J., et al. (2015). Sintering of lead-free piezoelectric sodium potassium niobate ceramics. Materials, 8(12): 8117-8146. https://doi.org/10.3390/ma8125449
[51] Han, G.S., Su, Y.F., Feng, Y.N., Lu, N. (2019). Approaches for increasing the β-phase concentration of electrospun polyvinylidene fluoride (PVDF) nanofibers. ES Materials and Manufacturing, 6: 75-80. https://doi.org/10.30919/esmm5f612
[52] He, Z., Rault, F., Lewandowski, M., Mohsenzadeh, E., Salaün, F. (2021). Electrospun PVDF nanofibers for piezoelectric applications: A review of the influence of electrospinning parameters on the β phase and crystallinity enhancement. Polymers, 13(2): 174. https://doi.org/10.3390/polym13020174
[53] Butt, M.A. (2022). Thin-film coating methods: A successful marriage of high-quality and cost-effectiveness-A brief exploration. Coatings, 12(8): 1115. https://doi.org/10.3390/coatings12081115
[54] Tsigara, A., Mourched, B., Falgayrettes, P., et al. (2014). Fabrication and mechanical properties of an organo-mineral cantilever-based probe for near-field optical microscopy. Sensors and Actuators A: Physical, 212: 12-17. https://doi.org/10.1016/j.sna.2014.03.016
[55] Mourched, B., Abdallah, M. (2022). Design and characterization of a new microscopy probe using COMSOL and ANSYS. The International Journal of Multiphysics, 16(1): 95-106. https://doi.org/10.21152/1750-9548.16.1.95
[56] Xia, Y., Zhou, X.Y., Niu, H.Z., Liu, H., Wu, C.W. (2025). Electric-mechanical coupling analysis of two-dimensional piezoelectric heterogeneous materials in flexible electric devices with extended multiscale isogeometric analysis. European Journal of Mechanics-A/Solids, 109: 105430. https://doi.org/10.1016/j.euromechsol.2024.105430
[57] Lefeuvre, E., Badel, A., Richard, C., Petit, L., Guyomar, D. (2006). A comparison between several vibration-powered piezoelectric generators for standalone systems. Sensors and Actuators A: Physical, 126(2): 405-416. https://doi.org/10.1016/j.sna.2005.10.043
[58] Ottman, G.K., Hofmann, H.F., Bhatt, A.C., Lesieutre, G.A. (2002). Adaptive piezoelectric energy harvesting circuit for wireless remote power supply. IEEE Transactions on Power Electronics, 17(5): 669-676. https://doi.org/10.1109/TPEL.2002.802194
[59] Badel, A., Guyomar, D., Lefeuvre, E., Richard, C. (2006). Piezoelectric energy harvesting using a synchronized switch technique. Journal of Intelligent Material Systems and Structures, 17(8-9): 831-839. https://doi.org/10.1177/1045389X06057533
[60] Nguyen, B.P., Tran, Q.H., Nguyen, T.T., Pradhan, A.M.S., Huynh, T.C. (2021). Understanding impedance response characteristics of a piezoelectric-based smart interface subjected to functional degradations. Complexity, 2021. https://doi.org/10.1155/2021/5728679
[61] He, Q., Briscoe, J. (2024). Piezoelectric energy harvester technologies: Synthesis, mechanisms, and multifunctional applications. ACS Applied Materials & Interfaces, 16(23): 29491-29520. https://doi.org/10.1021/acsami.3c17037
[62] Wang, Y.L., Yu, Y.N., Wei, X.Y., Narita, F. (2022). Self-powered wearable piezoelectric monitoring of human motion and physiological signals for the postpandemic era: A review. Advanced Materials Technologies, 7: 2200318. https://doi.org/10.1002/admt.202200318
[63] Mourched, B., Abboud, N., Abdallah, M., Moustafa, M. (2022). Electro-thermal simulation study of MOSFET modeling in silicon and silicon carbide. SSRN, 3972781. https://doi.org/10.2139/ssrn.3972781
[64] Wang, Z.L. (2013). Triboelectric nanogenerators as new energy technology for self-powered systems and as active mechanical and chemical sensors. ACS Nano, 7(11): 9533-9557. https://doi.org/10.1021/nn404614z
[65] Scott, M.D., Boser, B.E., Pister, K.S.J. (2003). An ultralow-energy ADC for smart dust. IEEE Journal of Solid-State Circuits, 38(7): 1123-1129. https://doi.org/10.1109/JSSC.2003.813296
[66] Banbury, C., Reddi, V.J., Torelli, P., et al. (2021). Mlperf tiny benchmark. arXiv preprint, arXiv:2106.07597. https://doi.org/10.48550/arXiv.2106.07597
[67] Nikodem, M., Bawiec, M. (2020). Experimental evaluation of advertisement-based bluetooth low energy communication. Sensors, 20(1): 107. https://doi.org/10.3390/s20010107
[68] Bulić, P., Kojek, G., Biasizzo, A. (2019). Data

transmission efficiency in Bluetooth Low Energy versions. Sensors, 19(17): 3746. https://doi.org/10.3390/s19173746
[69] Eaton. (2025). HS/HSL Supercapacitors: Hybrid Cylindrical Cells, Technical Data 11043. Eaton Corporation. https://www.eaton.com/content/dam/eaton/products/electronic-components/resources/data-sheet/eaton-supercapacitor-hybrid-cylindrical-cells-data-sheet.pdf.
[70] Rubab, N., Kim, S.W. (2022). Self-powered sensors based on piezoelectric nanogenerators. Journal of Sensor Science and Technology, 31(5). https://doi.org/10.46670/JSST.2022.31.5.293
[71] Ficco, M., Guerriero, A., Milite, E., Palmieri, F., Pietrantuono, R., Russo, S. (2024). Federated learning for IoT devices: Enhancing TinyML with on-board training. Information Fusion, 104(3): 102189. https://doi.org/10.1016/j.inffus.2023.102189
[72] Abdallah, M., Ferko, N., Neji, B., Vrtagic, S. (2022). Study and design of a machine learning-enabled laser-based sensor for pure and sea water determination using COMSOL Multiphysics. Applied Sciences (Switzerland), 12(13): 6693. https://doi.org/10.3390/app12136693
[73] Mourched, B., AlZoubi, T., Vrtagic, S. (2024). Diesel adulteration detection with a machine learning-enhanced laser sensor approach. Processes, 12(4): 798. https://doi.org/10.3390/pr12040798
[74] Mnif, M., Sahnoun, S., Kaaniche, M., Ben Atitallah, B., Fakhfakh, A., Kanoun, O. (2024). Ultra-fast edge computing approach for hand gesture classification based on EIT measurements. In 2024 IEEE International Symposium on Robotic and Sensors Environments (ROSE), Chemnitz, Germany, pp. 1-7. https://doi.org/10.1109/ROSE62198.2024.10591116
[75] Promsawat, M., Deluca, M., Kampoosiri, S., Marungsri, B., Pojprapai, S. (2017). Electrical fatigue behavior of lead zirconate titanate ceramic under elevated temperatures. Journal of the European Ceramic Society, 37(5): 2047-2055. https://doi.org/10.1016/j.jeurceramsoc.2016.12.037
[76] Selleri, G., Gino, M.E., Brugo, T.M., et al. (2022). Self-sensing composite material based on piezoelectric nanofibers. Materials & Design, 219: 110787. https://doi.org/10.1016/j.matdes.2022.110787
[77] Bhadwal, N., Ben Mrad, R., Behdinan, K. (2023). Review of zinc oxide piezoelectric nanogenerators: Piezoelectric properties, composite structures and power output. Sensors, 23(8): 3859. https://doi.org/10.3390/s23083859
[78] Yue, X.L., Javvaji, S., Tang, Z., Makinwa, K.A.A., Du, S.J. (2023). 30.3 a bias-flip rectifier with a duty-cycle-based MPPT algorithm for piezoelectric energy harvesting with 98% peak MPPT efficiency and 738% energy-extraction enhancement. In 2023 IEEE International Solid-State Circuits Conference (ISSCC), San Francisco, CA, USA, pp. 442-444. https://doi.org/10.1109/ISSCC42615.2023.10067284
[79] Covaci, C., Gontean, A. (2020). Piezoelectric energy harvesting solutions: A review. Sensors, 20(12): 3512. https://doi.org/10.3390/s20123512
[80] Iannicelli-Zubiani, E.M., Giani, M.I., Recanati, F., Dotelli, G., Puricelli, S., Cristiani, C. (2017). Environmental impacts of a hydrometallurgical process for electronic waste treatment: A life cycle assessment case study. Journal of Cleaner Production, 140: 1204-1216. https://doi.org/10.1016/j.jclepro.2016.10.040
[81] Li, F., Zhang, S.J., Yang, T.N., et al. (2016). The origin of ultrahigh piezoelectricity in relaxor-ferroelectric solid solution crystals. Nature Communications, 7: 13807. https://doi.org/10.1038/ncomms13807
[82] Kaltenbrunner, M., Sekitani, T., Reeder, J., et al. (2013). An ultra-lightweight design for imperceptible plastic electronics. Nature, 499(7459): 458-463. https://doi.org/10.1038/nature12314

NOMENCLATURE

S	Strain
T	Stress, $N.m^{-2}$
E	Electric field, $V.m^{-1}$
D	Electric displacement, $C.m^{-2}$
s^E	Elastic compliance at constant electric field, $m^2.N^{-1}$
d	Piezoelectric charge coefficient matrix (dt is its transpose), $C.N^{-1}$
d_{33}	Longitudinal piezoelectric charge coefficient, pC/N
d_{31}	Transverse piezoelectric charge coefficient, pC/N
d_{eff}	Effective piezoelectric coefficient, $C.N^{-1}$
g_{ij}, g_{33}	Piezoelectric voltage constants, $V.m.N^{-1}$
k	Electromechanical coupling factor
Q	Mechanical quality factor
Q	Generated electric charge, C
F	Applied force, N
C_p	Effective capacitance of the piezoelectric element, F
$E_{elec,max}$	Maximum stored electrostatic energy, J
E_{harv}	Electrical energy generated per operational cycle, J
E_{sense}	Energy required for sensing and data acquisition, J
E_{infer}	Energy required for embedded inference, J
E_{tx}	Energy required for wireless transmission, J
P_{harv}	Average harvested electrical power, W
$P_{harv,ideal}$	Idealized average transducer power, W
P_{usable}	Usable harvested power, W
P_{demand}	Total time-averaged power demand, W
P_{leak}	Storage and standby leakage power, W
f_{exc}	Excitation frequency, Hz
f_s	Sensing operation frequency, Hz
f_i	Inference operation frequency, Hz
f_t	Transmission operation frequency, Hz
$\mathcal{A}$	Autonomy ratio